INTERNATIONAL JOURNAL FOR NUMERICAL METHODS IN FLUIDS, VOL. 16, 187–198 (1993)

AN EFFICIENT THREE-DIMENSIONAL SEMI-IMPLICIT FINITE ELEMENT SCHEME FOR SIMULATION OF FREE SURFACE FLOWS

Y. S. LI AND J. M. ZHAN

Department of Civil and Structural Engineering, Hong Kong Polytechnic, Hung Hom, Kowloon, Hong Kong

SUMMARY

An efficient semi-implicit finite element model is proposed for the simulation of three-dimensional flows in stratified seas. The body of water is divided into a number of layers and the two horizontal momentum equations for each layer of water are first integrated vertically. Nine-node Lagrangian quadratic isoparametric elements are employed for spatial discretization in the horizontal domain. The time derivatives are approximated using a second-order-accurate semi-implicit time-stepping scheme. The distinguishing feature of the proposed numerical scheme is that only nodal values on the same vertical line are coupled. Two test cases for which analytic solutions are available are employed to test the proposed scheme. The test results show that the scheme is efficient and stable. A numerical experiment is also included to compare the proposed scheme with a finite difference scheme.

KEY WORDS Three-dimensional Finite element Free surface flows

1. INTRODUCTION

In coastal areas where salt water and fresh water meet, horizontal and vertical density gradients are produced. Also, upwelling sometimes occurs in coastal areas. Three-dimensional finite difference models have been extensively used in the last 20 years to simulate such flows. However, the use of three-dimensional finite element models to solve coastal flow problems is still scarce compared with the number of finite difference models available in the literature. In many applications the coastal configurations are very complicated and the ability of the finite element method to better represent arbitrary configurations should be exploited.

Koutitas and O'Connor[1] used a composite finite difference/finite element numerical procedure. The finite element Galerkin method was applied over depth using linear shape functions, while a finite difference approximation was employed for the horizontal domain. Signorini[2] used two-dimensional linear shape functions associated with three-node triangular elements for the horizontal domain. The vertical coupling between different levels was achieved by a finite difference scheme. Trösch[3] employed 20-node brick elements to compute the flow in a channel of constant depth with closed ends driven by wind. Although only 45 elements were used, the resulting set of simultaneous algebraic equations, after time discretization by an implicit finite difference scheme, had a total of 1080 degrees of freedom. The system matrix also had a large bandwidth, since each brick element had 68 degrees of freedom. Kawahara *et al.*[4] presented a multilayer finite element model with vertical integration applied to each water layer. The model was applied, using triangular elements, to study the current flow for regional development

0271–2091/93/030187–12$11.00

Received January 1992
Revised September 1992

planning analysis in Japan. Laible[5] used Hermitian polynomials involving the bottom and surface velocities and their gradients in the vertical direction to approximate the variation in flow velocities with depth. The wave equation model originally developed by Lynch and Gray[6] was then solved using nine-node Lagrangian quadratic isoparametric elements with integral lumping. This method was later extended to include two-layer flow systems.[7] Lynch and Werner[8] used six-node elements with linear triangles in the horizontal and linear variations in the vertical for the flow velocities and the surface elevation was solved using essentially a two-dimensional wave equation.

In this paper an efficient semi-implicit finite element model is proposed for the simulation of three-dimensional flows in stratified seas. The body of water is divided into a number of layers, the thicknesses of which can vary with depth. In addition, the thicknesses of the surface and bottom layers also vary horizontally owing to the variation in the sea level and in the bottom topography respectively. The two horizontal momentum equations for each layer of water are first integrated vertically so that only two-dimensional differential equations have to be solved. Nine-node Lagrangian quadratic isoparametric elements are then employed for spatial discretization in the horizontal domain. The time derivatives are approximated using a second-order-accurate semi-implicit time-stepping scheme. The distinguishing feature of the proposed numerical scheme is that only nodal values on the same vertical line are coupled and hence only a small set of simultaneous algebraic equations is required to be solved at each horizontal nodal point at each time step, which leads to a drastic reduction in computer time. Two test cases for which analytic solutions have been obtained are used to test the validity of the proposed scheme. Finally, a numerical experiment is included to compare the proposed scheme with a finite difference scheme.

2. GOVERNING DIFFERENTIAL EQUATIONS

The hydrodynamic equations can be written as

$$\frac{\partial u}{\partial t}+\frac{\partial (uu)}{\partial x}+\frac{\partial (vu)}{\partial y}+\frac{\partial (wu)}{\partial z}-fv+\frac{1}{\rho}\frac{\partial P}{\partial x}=\frac{1}{\rho}\left(\frac{\partial \tau_{xx}}{\partial x}+\frac{\partial \tau_{xy}}{\partial y}+\frac{\partial \tau_{xz}}{\partial z}\right), \tag{1}$$

$$\frac{\partial v}{\partial t}+\frac{\partial (uv)}{\partial x}+\frac{\partial (vv)}{\partial y}+\frac{\partial (wv)}{\partial z}+fu+\frac{1}{\rho}\frac{\partial P}{\partial y}=\frac{1}{\rho}\left(\frac{\partial \tau_{yx}}{\partial x}+\frac{\partial \tau_{yy}}{\partial y}+\frac{\partial \tau_{yz}}{\partial z}\right), \tag{2}$$

$$\frac{\partial u}{\partial x}+\frac{\partial v}{\partial y}+\frac{\partial w}{\partial z}=0, \tag{3}$$

where u, v and w are the x-, y- and z-components of current respectively in Cartesian co-ordinates, with z, the vertical co-ordinate, increasing upwards, ρ is the density of water, P is the pressure, f is the Coriolis parameter, which is twice the value of the vertical component of the Earth's rotation, and τ_{ij} are interfacial shear stresses.

The pressure distribution in the vertical is assumed to be hydrostatic:

$$P=P_0+\rho_L g(\eta-z)+I, \tag{4}$$

where η is the water surface elevation above the reference datum, P_0 is atmospheric pressure, ρ_L is the density of water on the free surface and I is the baroclinic pressure component.

The body of water is divided into a number of layers (see Figure 1) and the following notations are used:

$$U_k=\int_{z_k}^{z_{k+1}} u\,dz, \qquad V_k=\int_{z_k}^{z_{k+1}} v\,dz, \tag{5}$$

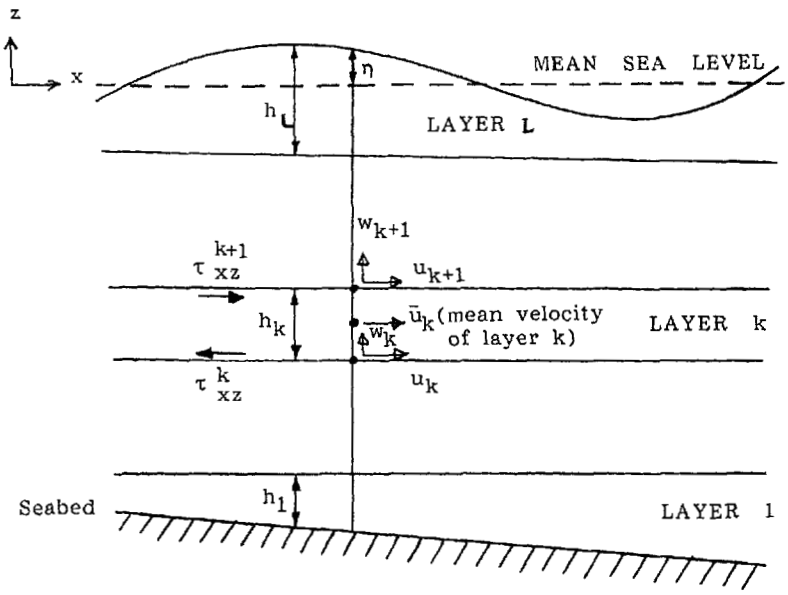

Figure 1. Vertical arrangement of grid points in an x–z section

i.e. U_k and V_k are the discharges per unit width in the x- and y-directions respectively of layer k.

The following approximations usually employed in 2D flow models are used:

$$\int_{z_k}^{z_{k+1}} u^2 \mathrm{d}z = \frac{U_k U_k}{h_k}, \qquad \int_{z_k}^{z_{k+1}} uv \mathrm{d}z = \frac{U_k V_k}{h_k}, \qquad \int_{z_k}^{z_{k+1}} v^2 \mathrm{d}z = \frac{V_k V_k}{h_k}, \tag{6}$$

where $h_k = z_{k+1} - z_k$ is the thickness of the kth layer.

The vertically integrated form of the momentum equations (1) and (2) for each layer, incorporating the above approximations, are

$$\frac{\partial U_k}{\partial t} + \frac{\partial}{\partial x}\left(\frac{U_k U_k}{h_k}\right) + \frac{\partial}{\partial y}\left(\frac{U_k V_k}{h_k}\right) + u_{k+1} w_{k+1} - u_k w_k - f V_k$$
$$+ \frac{h_k}{\rho_k}\frac{\partial}{\partial x}(P_0 + \rho_L g\eta + I_k) - \frac{1}{\rho_k}\left[(\tau_{xz}^{k+1} - \tau_{xz}^{k}) + \rho_k \nu\left(\frac{\partial^2 U_k}{\partial x^2} + \frac{\partial^2 U_k}{\partial y^2}\right)\right] = 0, \tag{7}$$

$$\frac{\partial V_k}{\partial t} + \frac{\partial}{\partial x}\left(\frac{U_k V_k}{h_k}\right) + \frac{\partial}{\partial y}\left(\frac{V_k V_k}{h_k}\right) + v_{k+1} w_{k+1} - v_k w_k + f U_k$$
$$+ \frac{h_k}{\rho_k}\frac{\partial}{\partial y}(P_0 + \rho_L g\eta + I_k) - \frac{1}{\rho_k}\left[(\tau_{yz}^{k+1} - \tau_{yz}^{k}) + \rho_k \nu\left(\frac{\partial^2 V_k}{\partial x^2} + \frac{\partial^2 V_k}{\partial y^2}\right)\right] = 0, \tag{8}$$

where ν is the horizontal eddy viscosity.

The following assumptions about τ_{xz} and τ_{yz} are made:

$$\tau_{xz}^k = \left(\rho\varepsilon\frac{\partial u}{\partial z}\right)^k = \frac{\rho_k \varepsilon_k}{(h_{k-1} + h_k)/2}(\bar{u}_k - \bar{u}_{k-1}) = \frac{2\rho_k \varepsilon_k}{h_{k-1} + h_k}\left(\frac{U_k}{h_k} - \frac{U_{k-1}}{h_{k-1}}\right), \tag{9}$$

where $\bar{u}_{k-1}$ and $\bar{u}_k$ are the mean velocities of layers $k-1$ and k respectively and ε_k is the vertical eddy viscosity. A similar expression is used for τ_{yz}^k.

The bottom stress components are assumed to be of the following form:

$$\tau_{xz}^1=\rho_1\alpha S U_1, \qquad \tau_{yz}^1=\rho_1\alpha S V_1, \tag{10}$$

where $S=\sqrt{[U_1^2+V_1^2]}/h_1^2$ and α is the friction parameter.

Besides using slip conditions, an alternative no-slip bottom boundary condition can be used. The surface stress components τ_{xz}^{L+1} and τ_{yz}^{L+1} are known functions of x, y and t.

Integration of the continuity equations (3) gives

$$w_k=-\sum_{i=1}^{k-1}\left(\frac{\partial U_i}{\partial x}+\frac{\partial V_i}{\partial y}\right), \qquad k=2,\ldots,L. \tag{11}$$

In the present calculations the vertical eddy viscosity is assumed to be of constant value.

The boundary conditions are zero flow normal to a solid boundary and specified water surface elevation or normal flow velocities of all layers at an open boundary.

3. FINITE ELEMENT FORMULATION

The strategy adopted to reduce the computation time is to expand each term of the governing equations (7) and (8) for each layer as previously applied to the simulations of 2D flows, rather than each dependent variable, in terms of the unknown nodal values.[9] Some typical expansions are given below:

$$U_1=\sum_{j=1}^{N}\Phi_j(x,y)U_1^j(t), \qquad \frac{U_1U_1}{h_1}=\sum_{j=1}^{N}\Phi_j(x,y)\left(\frac{U_1U_1}{h_1}\right)^j(t), \tag{12a}$$

$$V_1=\sum_{j=1}^{N}\Phi_j(x,y)V_1^j(t), \qquad \frac{U_1V_1}{h_1}=\sum_{j=1}^{N}\Phi_j(x,y)\left(\frac{U_1V_1}{h_1}\right)^j(t), \tag{12b}$$

$$u_2w_2=\sum_{j=1}^{N}\Phi_j(x,y)(u_2w_2)^j(t), \qquad S=\sum_{j=1}^{N}\Phi_j(x,y)S^j(t), \tag{12c}$$

$$\frac{2\varepsilon_2}{h_1+h_2}\frac{U_2}{h_2}=\sum_{j=1}^{N}\Phi_j(x,y)\left(\frac{2\varepsilon_2}{h_1+h_2}\frac{U_2}{h_2}\right)^j(t), \tag{12d}$$

$$\frac{2\varepsilon_2}{h_1+h_2}\frac{U_1}{h_1}=\sum_{j=1}^{N}\Phi_j(x,y)\left(\frac{2\varepsilon_2}{h_1+h_2}\frac{U_1}{h_1}\right)^j(t), \tag{12e}$$

$$\eta=\sum_{j=1}^{N}\Phi_j(x,y)\eta^j(t), \qquad \frac{h_1}{\rho_1}=\sum_{j=1}^{N}\Phi_j(x,y)\left(\frac{h_1}{\rho_1}\right)^j(t), \tag{12f}$$

$$P_0=\sum_{j=1}^{N}\Phi_j(x,y)P_0^j(t), \qquad I_1=\sum_{j=1}^{N}\Phi_j(x,y)I_1^j(t). \tag{12g}$$

Substitution of the finite element approximations given above into equation (7) for layer 1 yields the following element matrix equation for an element A_e after application of the Galerkin criterion:

$$A\left\{\frac{dU_1}{dt}\right\}+B\left\{\frac{U_1U_1}{h_1}\right\}+C\left\{\frac{U_1V_1}{h_1}\right\}+A\{u_2w_2\}-fA\{V_1\}+\rho_L gD\{\eta\}+D\{P_0\}$$
$$+D\{I_1\}-A\left\{\frac{2\varepsilon_2}{h_1+h_2}\frac{U_2}{h_2}\right\}+A\left\{\frac{2\varepsilon_2}{h_1+h_2}\frac{U_1}{h_1}\right\}+\alpha E\{U_1\}+G1\{U_1\}+G2\{U_1\}=0, \tag{13}$$

where A, B, C, D, E, $G1$ and $G2$ are $N \times N$ matrices, with

$$A_{i,j} = \iint_{A_e} \Phi_i \Phi_j \mathrm{d}x\mathrm{d}y, \qquad B_{i,j} = \iint_{A_e} \Phi_i \frac{\partial \Phi_j}{\partial x} \mathrm{d}x\mathrm{d}y, \tag{14a}$$

$$C_{i,j} = \iint_{A_e} \Phi_i \frac{\partial \Phi_j}{\partial y} \mathrm{d}x\mathrm{d}y, \qquad D_{i,j} = \sum_{m=1}^{N} \iint_{A_e} \Phi_m \left(\frac{h_1}{\rho_1}\right)^m \Phi_i \frac{\partial \Phi_j}{\partial x} \mathrm{d}x\mathrm{d}y, \tag{14b}$$

$$E_{i,j} = \sum_{m=1}^{N} \iint_{A_e} \Phi_m S^m \Phi_i \Phi_j \mathrm{d}x\mathrm{d}y, \quad G1_{i,j} = \iint_{A_e} \nu \frac{\partial \Phi_i}{\partial x} \frac{\partial \Phi_j}{\partial x} \mathrm{d}x\mathrm{d}y, \tag{14c}$$

$$G2_{i,j} = \iint_{A_e} \nu \frac{\partial \Phi_i}{\partial y} \frac{\partial \Phi_j}{\partial y} \mathrm{d}x\mathrm{d}y, \tag{14d}$$

and $\{\ \}$ denotes a column vector.

The line integral resulting from the integration of the momentum equation does not appear in (13), because all the turbulent stresses τ_{xx}, τ_{xy}, τ_{yx} and τ_{yy} are assumed to be negligible at the open boundary in the present model.

Similar equations can be obtained for V_1, U_2, $V_2, \ldots, U_L$ and V_L. In this scheme, Lagrangian quadratic isoparametric elements with nine nodes are used. Following Gray and van Genuchten,[10] numerical integrations are carried out using Simpson's rule. The coincidence of the nine integration points of Simpson's rule with the nine nodes of the Lagrangian quadratic isoparametric elements greatly enhances the computational efficiency. Since Φ_i has a value of unity at node i and is zero at all other nodes, $\Phi_i \Phi_j$ is zero at the integration points unless $i = j$ and thus A and E are diagonal matrices.

The vertical velocity w_k can be obtained from the continuity equation (3) after vertical integration as follows:

$$A\{w_k\} = -\sum_{i=1}^{k-1} (B\{U_i\} + C\{V_i\}). \tag{15}$$

Equation (13) is now finite differenced in the time domain by a semi-implicit one-step method as follows:

$$\begin{aligned} &A\left\{\frac{U_1^{t+\Delta t} - U_1^{t-\Delta t}}{2\Delta t}\right\} + B\left\{\left(\frac{U_1 U_1}{h_1}\right)^t\right\} + C\left\{\left(\frac{U_1 V_1}{h_1}\right)^t\right\} + A\{(u_2 w_2)^t\} - fA\left\{\frac{V_1^{t+\Delta t} + V_1^{t-\Delta t}}{2}\right\} \\ &\quad + \rho_L g D^t\{\eta^t\} + D(P_0^t\} + D\{I_1^t\} - \frac{A}{2}\left\{\left(\frac{2\varepsilon_2}{h_1+h_2}\frac{U_2}{h_2}\right)^{t+\Delta t} + \left(\frac{2\varepsilon_2}{h_1+h_2}\frac{U_2}{h_2}\right)^{t-\Delta t}\right\} \\ &\quad + \frac{A}{2}\left\{\left(\frac{2\varepsilon_2}{h_1+h_2}\frac{U_1}{h_1}\right)^{t+\Delta t} + \left(\frac{2\varepsilon_2}{h_1+h_2}\frac{U_1}{h_1}\right)^{t-\Delta t}\right\} + \alpha E^t\left\{\frac{U_1^{t+\Delta t} + U_1^{t-\Delta t}}{2}\right\} + G1\{U_1^t\} + G2\{U_1^t\} = 0. \end{aligned} \tag{16}$$

Since the stress terms between layers, $\{2\varepsilon_2 U_2/h_2(h_1+h_2)\}$ and $\{2\varepsilon_2 U_1/h_1(h_1+h_2)\}$, the Coriolis term $f\{V_1\}$ and the bottom friction term $\alpha\{U_1\}$ in equation (13) are associated with a diagonal matrix (A or E) in addition to $\{\mathrm{d}U_1/\mathrm{d}t\}$, they are also represented semi-implicitly in equation (16). The semi-implicit representation of the stress terms between layers and the bottom friction term will greatly enhance the computational stability. The implicit representation of the Coriolis term will also improve the computational stability if the numerical model is applied to simulate large-scale flows. The same time-stepping scheme is applied to the other ordinary differential equations for V_1, U_2, $V_2, \ldots, U_L$ and V_L.

Since A and E are both diagonal matrices, only nodal values on the same vertical line are coupled and hence only a small set of simultaneous algebraic equations is required to be solved at each horizontal nodal point. Knowing $U_k^{t+\Delta t}$ and $V_k^{t+\Delta t}$, the water surface elevation $\eta^{t+\Delta t}$ can be solved from

$$A\left\{\frac{\eta^{t+\Delta t}-\eta^t}{\Delta t}\right\}+B\left\{\frac{\sum_{k=1}^{L}(U_k^{t+\Delta t}+U_k^t)}{2}\right\}+C\left\{\frac{\sum_{k=1}^{L}(V_k^{t+\Delta t}+V_k^t)}{2}\right\}=0. \tag{17}$$

4. VERIFICATION OF THE NUMERICAL SCHEME

4.1. Numerical experiment 1: flow in a rectangular channel

This numerical experiment is concerned with the simulation of a steady two-dimensional, wind-induced flow in a uniform rectangular channel of length 1000 m, width 400 m and depth $h=10$ m. The free surface is acted on by a constant wind-induced stress $\tau_{xz}^{L+1}=1{\cdot}5\ \mathrm{N\,m^{-2}}$ as shown in Figure 2. The water body was divided into eight equal layers and the following parameters were adopted: $\Delta x=\Delta y=100$ m; $\Delta t=5$ s; $v=0$; $f=0$; $\rho=1025\ \mathrm{kg\,m^{-3}}$.

Using the no-slip condition at the channel bed, the following uniform and steady state analytic solution for a well-mixed channel with constant vertical eddy viscosity ε was known:[1]

$$u=\tau_{xz}^{L+1}\,\sigma(h+\eta)(3\sigma-2)/4\varepsilon\rho, \quad \text{where } \sigma=(h+z)/(h+\eta).$$

The computed steady state vertical velocity profiles at the mid-length of the channel, where the free surface elevation, is zero and the corresponding analytic solutions for two different values of the vertical eddy viscosity ε are shown in Figures 3(a) and 3(b). It can be seen that the computed results agree very well with the analytic solutions.

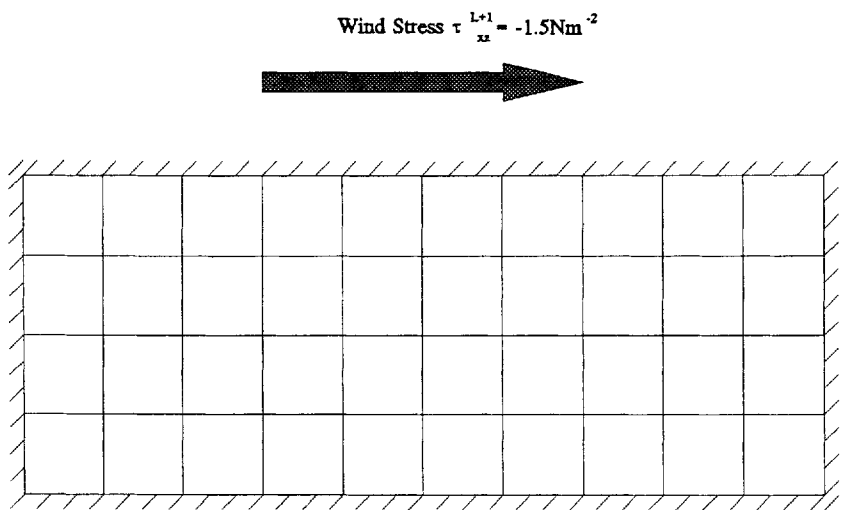

Figure 2. Geometry and horizontal mesh used in numerical experiment 1

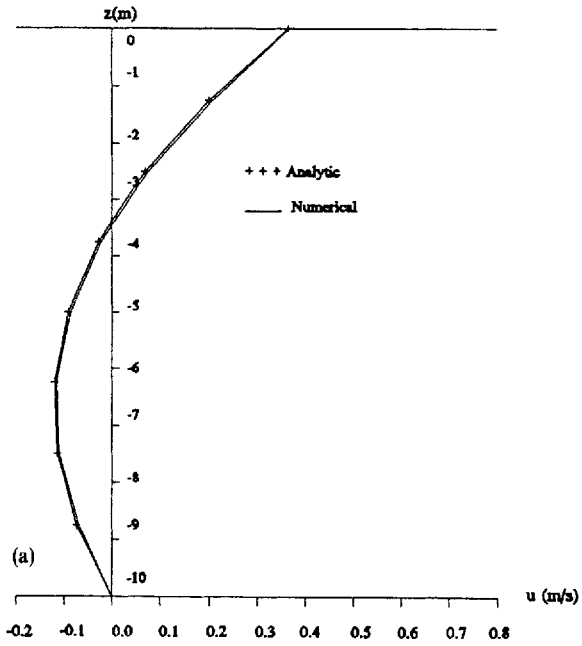

Figure 3(a). Comparison of analytic and computed u-velocity profiles for flow in a rectangular channel with $\varepsilon = 0{\cdot}01\ \mathrm{m^2\,s^{-1}}$

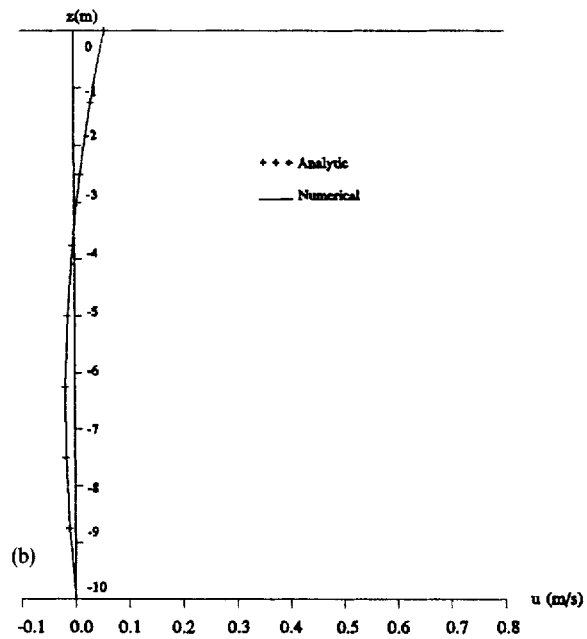

Figure 3(b). Comparison of analytic and computed u-velocity profiles for flow in a rectangular channel with $\varepsilon = 0{\cdot}065\ \mathrm{m^2\,s^{-1}}$

4.2. Numerical experiment 2: flow in an annular section

This numerical experiment is concerned with the three-dimensional flow in an annular section driven by tidal forcing at the open boundary with angular frequency $\omega = 1{\cdot}41 \times 10^{-4}\ s^{-1}$ (period 12·4 h). The problem geometry and the horizontal mesh are shown in Figure 4. The water depth

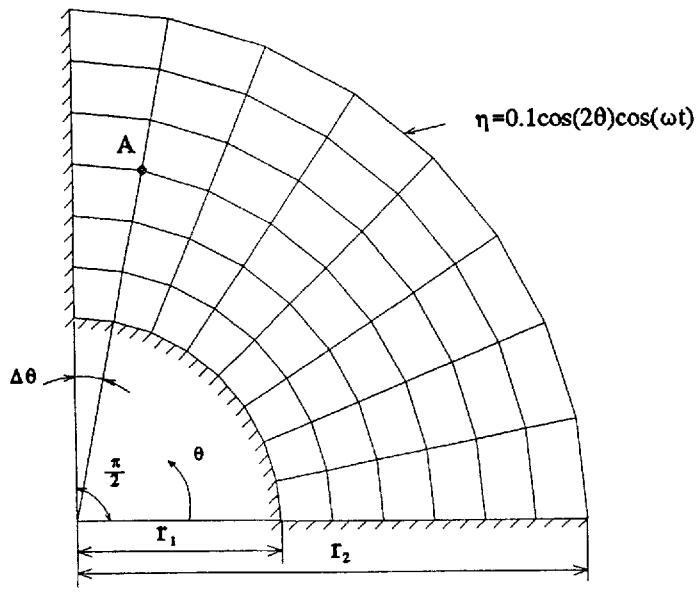

Figure 4. Geometry and horizontal mesh used in numerical experiment 2

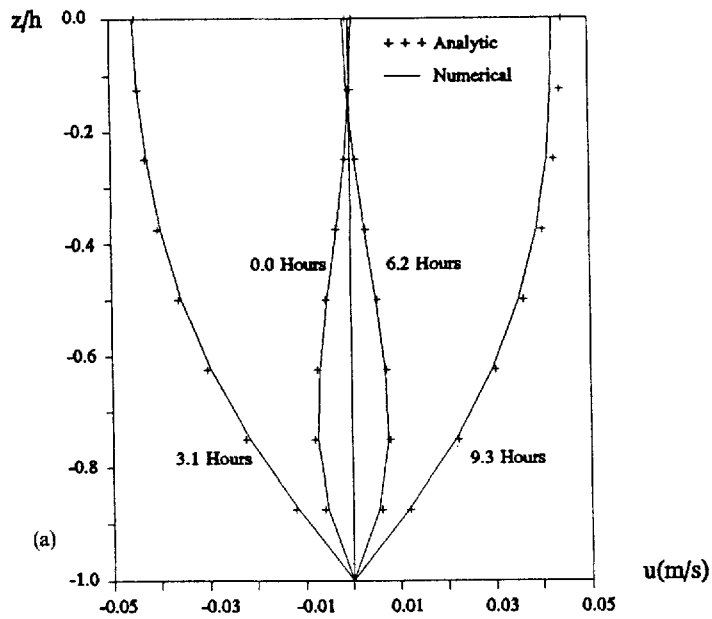

Figure 5(a). Comparison of analytic and computed u-velocity profiles for flow in an annular section

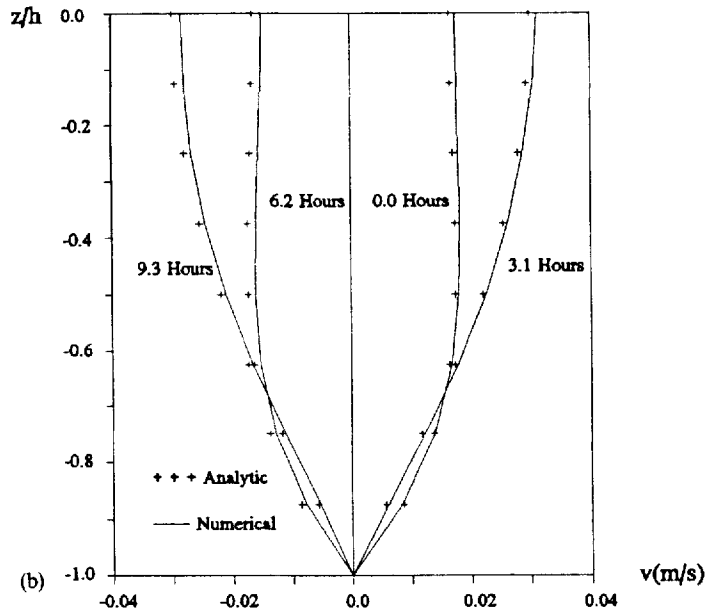

Figure 5(b). Comparison of analytic and computed v-velocity profiles for flow in an annular section

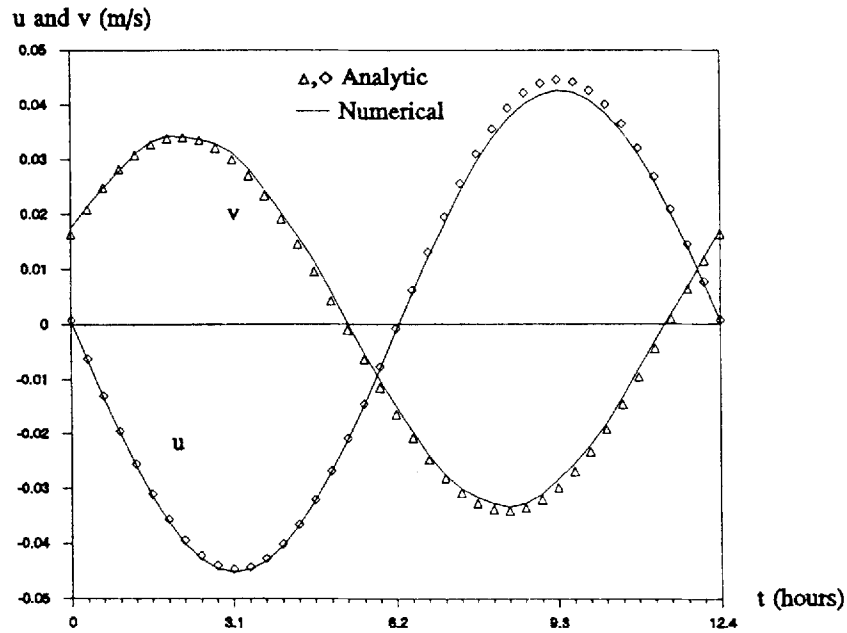

Figure 6. Comparison of variations of analytic and computed surface velocities at point A over one tidal cycle

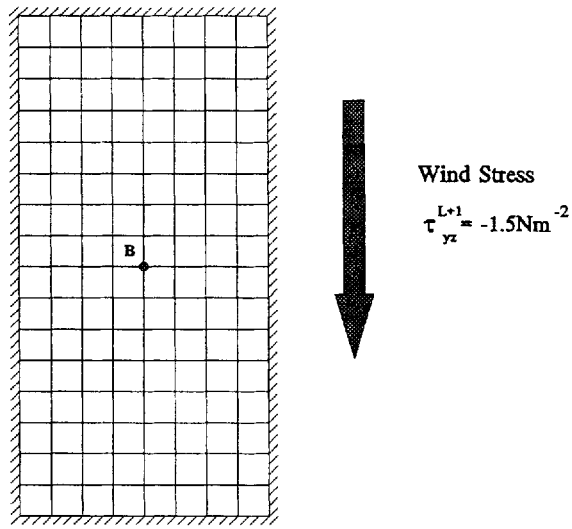

Figure 7. Geometry and horizontal mesh used in numerical experiment 3

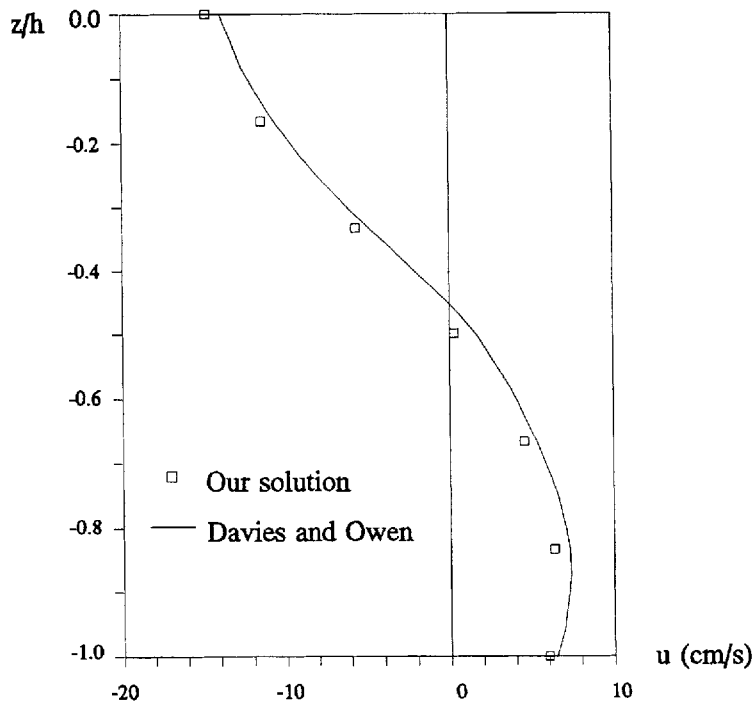

Figure 8(a). Comparison of computed u-velocity profiles for flow in a closed rectangular basin

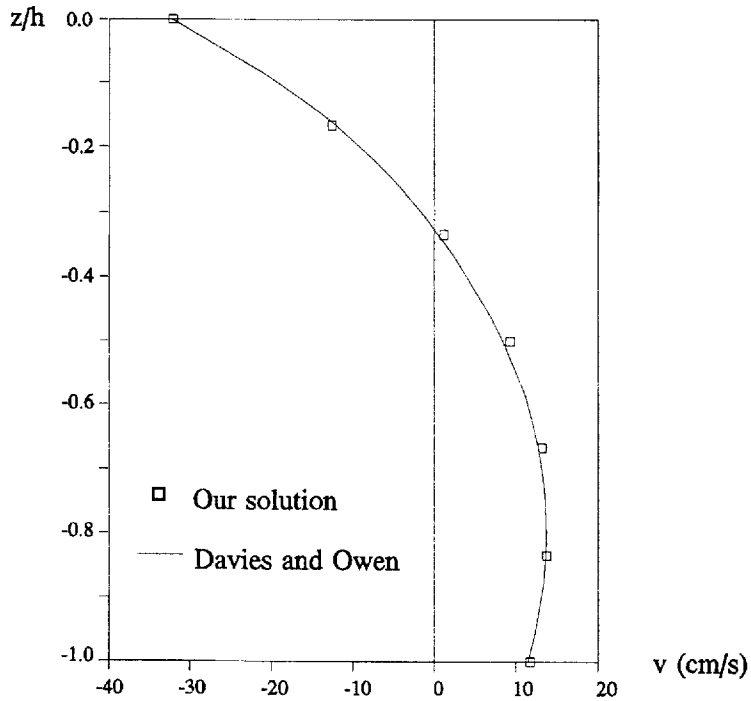

Figure 8(b). Comparison of computed v-velocity profiles for flow in a closed rectangular basin

h varied quadratically with r and a sufficiently large bottom stress coefficient was employed to enforce no slip at the bottom. The water body was divided into eight equal layers and the following parameters were adopted: $\Delta\theta = \pi/16$ rad; $\Delta t = 279$ s; $\tau_{xz}^{L+1} = \tau_{yz}^{L+1} = f = v = 0$; $h = h_0 r^2$, with $h_0 = 3{\cdot}048 r_1^{-2}$ m^{-1}; $r_1 = 60\,960$ m; $r_2 = 152\,400$ m; $\omega h^2/\varepsilon = 10$; surface elevation at r_2 taken as $\eta = 0{\cdot}1 \cos(2\theta) \cos(\omega t)$; linear bottom friction parameter $\alpha S = 10$ m s^{-1}.

The linearized analytic solution for this test case can be obtained using the method given in Reference 11. The computed vertical velocity profiles at mesh point A together with the analytic solutions at four points in time are shown in Figures 5(a) and 5(b). The time variations of the analytic and computed surface velocity components at point A over one tidal cycle are depicted in Figure 6. It can be seen that the agreement with the analytic solution is very good in all cases.

4.3. Numerical experiment 3: flow in a closed rectangular basin

This numerical experiment is concerned with the simulation of three-dimensional wind-induced flow in a rectangular basin with dimensions and rotation representative of the North Sea as considered by Davies and Owen[12] (see Figure 7). The water initially at rest was subject to a uniform wind stress of 1·5 N m^{-2} in the direction of decreasing y, corresponding to a north wind blowing over the North Sea. The water body was divided into six equal layers and the following parameters were adopted: $\Delta x = 400$ km/8; $\Delta y = 800$ km/16; $h = 65$ m; $\rho = 1025$ kg m^{-3}; $f = 0{\cdot}44$ h^{-1}; $v = 0$; $\Delta t = 100$ s; $\varepsilon = 0{\cdot}065$ m^2 s^{-1}; linear bottom friction parameter $\alpha S = 0{\cdot}002$ m s^{-1}.

The computed vertical velocity profiles at the centre of the basin (point B in Figure 7) 75 h after the onset of the wind field are shown in Figures 8(a) and 8(b) together with the computed

solutions by Davies and Owen.[12] It can be observed that the two sets of computed results agree very well.

5. CONCLUSIONS

The usefulness of the proposed semi-implicit finite element scheme for three-dimensional free surface flow computations has been established by using systematic test problems. Since only nodal values on the same vertical line are coupled, the computer execution time is greatly reduced. Application of the proposed scheme to prototype flow simulations and verification of the computed results with field data are required before the scheme can be fully established and used for predictive purposes with confidence. This is now under investigation and will be reported in a future paper.

ACKNOWLEDGEMENTS

This work was jointly supported by research grants from the Hong Kong Polytechnic and the Hong Kong Research Grant Council and was performed while the second author was a visiting researcher from the Department of Applied Mechanics and Engineering, Zhongshan University, China.

REFERENCES

1. C. Koutitas and B. O'Connor, 'Modelling three-dimensional wind-induced flows', *J. Hydraul. Div., ASCE*, **106,** 1843–1865 (1980).
2. S. R. Signorini, 'A three-dimensional numerical model of circulation and diffusion–advection processes for estuarine and coastal application by finite-element method', in T. Kawai (ed.), *Finite Element Flow Analysis*, University of Tokyo Press, Tokyo, 1982, pp. 603–610.
3. J. Trösch, 'Three-dimensional finite element for the calculations of circulations in a deep lake', in T. Kawai (ed.), *Finite Element Flow Analysis*, University of Tokyo Press, Tokyo, 1982, pp. 529–534.
4. M. Kawahara, M. Kobayashi and K. Nakata, 'A three-dimensional multiple level finite element method considering variable water density', in R. H. Gallagher, D. H. Norrie, J. T. Oden and O. C. Zienkiewicz (eds), *Finite Elements in Fluids*, Vol. 4, Wiley, Chichester, 1982, pp. 129–156.
5. J. P. Laible, 'A modified wave equation model for 3D flow in shallow bodies of water', in J. P. Laible, C. A. Brebbia, W. Gray and G. Pinder (eds), *Finite Elements in Water Resources*, Springer, Berlin, 1984, pp. 609–620.
6. D. R. Lynch and W. G. Gray, 'A wave equation model for finite element tidal computations', *Comput. Fluids*, **7,** 207–228 (1979).
7. J. P. Laible, 'A layered wave equation model for thermally stratified flow', in M. A. Celia, L. A. Ferrand, C. A. Brebbia, W. G. Gray and G. F. Pinder (eds), *Developments in Water Science*, Vol. 35, Elsevier, Amsterdam, 1988, pp. 319–327.
8. D. R. Lynch and F. E. Werner, 'Three-dimensional hydrodynamics on finite elements. Part II: Non-linear time-stepping model', *Int. j. numer. methods fluids*, **12,** 507–533 (1991).
9. L. G. Chen, Y. S. Li and K. K. Wong, 'An efficient semi-implicit finite element scheme for two-dimensional tidal flow computations', *Comput. Mech.*, **5,** 161–173 (1989).
10. W. G. Gray and M. Th. van Genuchten, 'Economical alternatives to Gaussian quadrature over isoparametric quadrilaterals', *Int. j. numer. methods eng.*, **12,** 1478–1484 (1978).
11. D. R. Lynch and C. B. Officer, 'Analytic test cases for 3-D hydrodynamics models', *Int. j. numer. methods fluids*, **5,** 529–543 (1985).
12. A. M. Davies and A. Owen, 'Three dimensional numerical sea model using the Galerkin method with a polynomial basis set', *Appl. Math. Modell.*, **3,** 421–428 (1979).